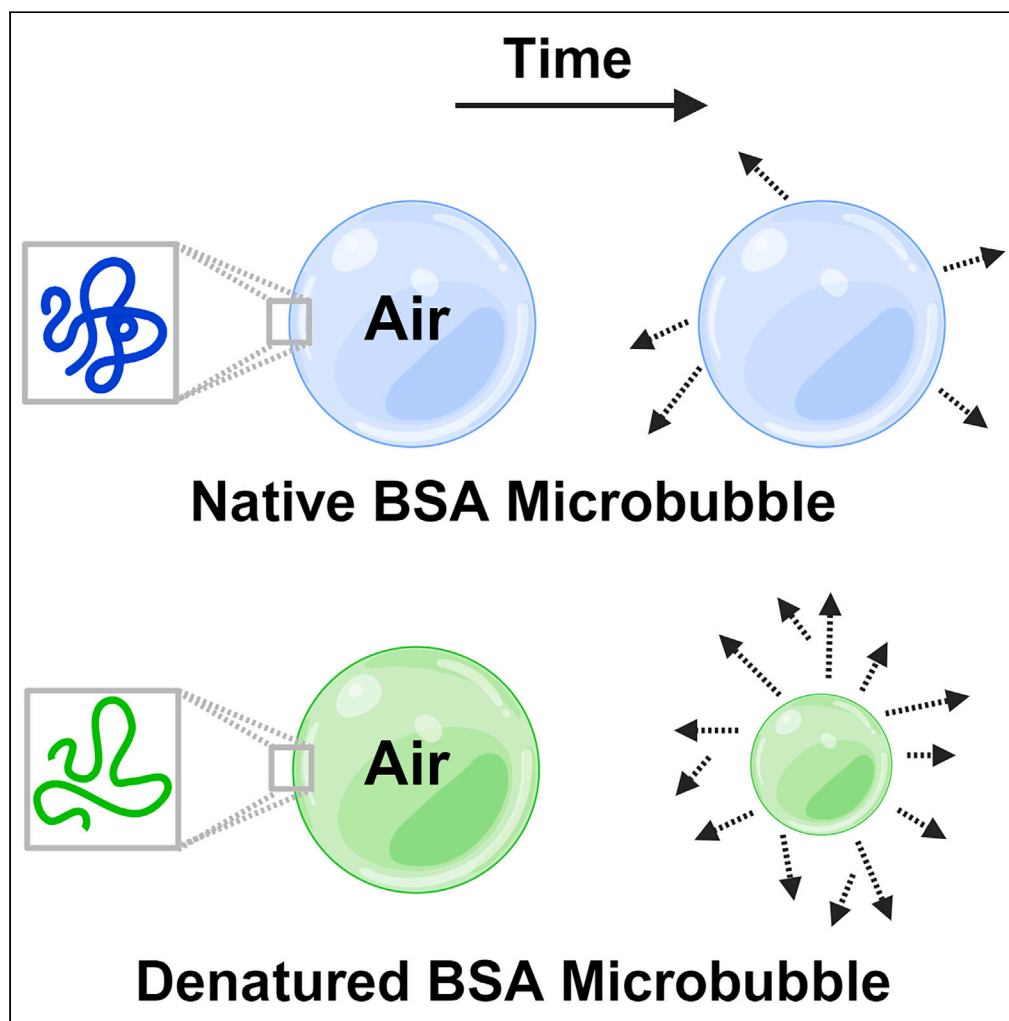**Article**

Influence of protein nativity on the stability of bovine serum albumin coated microbubbles

Palash Dhara,
Niyati Shah, Vidya
Sundaram, ...,
Yongfeng Mei,
Dmitry A. Gorin,
Krishna Kanti Dey

k.dey@iitgn.ac.in

Highlights

Native protein-shelled
microbubbles are more
stable than their denatured
counterparts

With denaturation, radius
of gyration and void
volumes of protein
molecules increase

Experimental results are
supported with
computational and
analytical studies

The results are expected to
find key implications in
targeted transport and
delivery

Article

Influence of protein nativity on the stability of bovine serum albumin coated microbubbles

Palash Dhara,[1,5] Niyati Shah,[1,5] Vidya Sundaram,[2] Ashutosh Srivastava,[2] Alexander A. Solovev,[3] Yongfeng Mei,[3] Dmitry A. Gorin,[4] and Krishna Kanti Dey[1,6,*]

SUMMARY

Protein-coated microbubbles have become one of the emerging platforms in biomedical research as theranostic agents. In recent years, microbubbles have been extensively used as ultrasound contrast agents and carriers of molecular cargoes, pertaining to which several studies have focused on tuning the properties of these bubbles to achieve a higher degree of biocompatibility and extended stability. Synthesis of microbubbles has so far been traditionally carried out with pre-heated proteins like bovine serum albumin (BSA) as shell coatings, owing to the ease in making BSA crosslinked structures through disulfide bridge formation. We, however, have performed experiments to demonstrate that air core microbubbles formed with native BSA are more stable compared with those formed using denatured BSA. The experimental observations have been supported with analytical modeling and computational studies, which offer insights into the effect of BSA conformation in stabilizing the microbubbles shells and prolonging their lifetimes.

INTRODUCTION

Microbubbles are small, gas core bubbles that have their sizes in the micron range. With the discovery that they can be used *in vivo* as ultrasound contrast agents,[1] the number of studies on microbubbles and the range of their applications have only increased since. Due to their unique dynamics under ultrasound, which includes oscillations, non-linear responses, microstreaming, and shell rupture, they are also being probed as targeted drug delivery agents and sensors in cancers, tumors, and neurodegenerative diseases.[2–5] With the rise in the number of possible *in vivo* applications, various studies on microbubbles have also focused on creating biocompatible bubbles with greater degrees of stability. Microbubbles are often coated with materials such as proteins, lipids, polymers, surfactants, etc., which can form crosslinked meshes, reduce surface tension, and provide a barrier against gas leakage.[3] The reduction in Laplace pressure across the microbubble surface prolongs their lifetimes. Apart from the properties of the shell material, microbubble stability also depends on the type of core gas and the environment in which they are stored.[6] High-molecular-weight gases like sulfur hexafluoride, perfluorocarbon, etc., which do not readily dissolve in water, when used as core gases, lead to enhanced lifetimes of the bubbles.[6]

There have been a few interesting studies carried out by different research groups to understand the dissolution dynamics of microbubbles.[7–9] External additives such as polyethylene glycol (PEG),[10] tryptophan (Tryp),[11] etc. have been used to prolong the shelf lives of microbubbles and increase their biocompatibility. However, for advanced *in vivo* usage of microbubbles, studies also need to be carried out to understand the integrability and immunogenic responses triggered within the host upon microbubble administration. Due to the complex and challenging nature of such studies, it is desirable to have easy fabrication protocols for bubbles with minimum surface functionalization strategies that could lead to their enhanced stability and prolonged circulation times. In this direction, stability of microbubbles modulated by their inherent shell features will not only help in attaining easy and resource-efficient fabrication methodologies but will also enable us to regulate and predetermine their lifetimes. The present study aims to contribute toward this end by demonstrating microbubble stability controlled by the degree of nativity of their shell-forming proteins.

Traditional synthesis protocols[12] for protein-shelled microbubbles involve- the use of probe sonicators or high-frequency mixers and cysteine-containing proteins such as bovine serum albumin (BSA), human serum albumin (HSA), and hemoglobin (Hb). Among these, molecules of pre-heated BSA have been used extensively in protein microbubble synthesis as these are robust, readily available, and relatively inexpensive. Details of a few important studies on microbubbles synthesis with pre-heated BSA have been highlighted in Table 1.

[1]Laboratory of Soft and Living Materials, Department of Physics, Indian Institute of Technology Gandhinagar, Palaj, Gandhinagar, Gujarat 382055, India
[2]Department of Biological Sciences and Engineering, Indian Institute of Technology Gandhinagar, Palaj, Gandhinagar, Gujarat 382055, India
[3]Department of Materials Science, Fudan University, Shanghai 200433 P.R. China
[4]Center for Photonics Sciences and Engineering, Skolkovo Institute of Science and Technology, 3 Nobelya Str., 121205 Moscow, Russia
[5]These authors contributed equally
[6]Lead contact
*Correspondence: k.dey@iitgn.ac.in
https://doi.org/10.1016/j.isci.2024.109286

Table 1. Comparison of experimental conditions and stabilities of various reported BSA-shelled microbubble formulations

| BSA concentration	Sonication conditions	Lifetime at 4°C	Lifetime at room temperature	Reference
5% BSA, pH 7	Air and Ar gas, 3 min, 200 W/cm^2, pre-heating temperature 50°C	Not reported	Not reported	Grinstaff and Suslick[12]
5% BSA, pH 7	Air, 3 min, 150 W, pre-heating temperature not mentioned	Several months	Several days	Suslick et al.[13]
5% BSA and 4 mM octanoic acid in phosphate-buffered saline (PBS)	Oxygen gas, pre-heated at 65°C, sonication chamber maintained at 75°C	Initial microbubble sizes were nearly 3 μm, which reduced to 1–2 μm in 12 days	Not reported	Swanson and Borden[14]
5% BSA +5% dextrose	n-decafluorobutane gas, 70–80 s, 450 W	At 5°C, microbubbles were stable for more than a year. Air-dried bubbles were stable for 2 years	Not reported	Borrelli et al.[15]
30 mg/mL BSA	Perfluorobutane (PFB) gas, pre-heated at 72°C, sonicated for ∼8–10 s at 105 W (100% amplitude)	<30 days in original solution and PGO (PGO: 10% 1,2-propane-diol, 10% glycerol, 80% BSA+CA+Tryp)	20 min in PBS at 37°C	Upadhyay and Dalvi[11]
BSA +0.98 mg/mL N-acetyl-DL-tryptophan (Tryp)		<30 days in original solution and ∼8 months in PGO	>30 min in PBS at 37°C	
BSA +0.634 μL/mL caprylic acid (CA)		<30 days in original solution and PGO	20 min in PBS at 37°C	
BSA+CA+Tryp		<30 days in original solution	30 min in PBS at 37°C	
5% BSA, pH 6, ionic strength 0.05 M	Air, 3 min, 30% amplitude, pre-heating at 55°C	>70 days	∼30 days at 20°C–25°C	Rovers et al.[16]
BSA (50 mg in 0.75 mL) in ethylenediaminetetraacetic acid (EDTA)-PBS + Traut's reagent	Air, pre-heating at 45°C for 10 min, 45 s, 173 W (23% amplitude)	Several months	Not reported	Ma et al.[17]
BSA (30 mg/mL) + 9.8 mg/mL N-acetyl-DL-tryptophan (Tryp)	PFB gas, 8–10 s, 100% amplitude, preheated at 71°C	1 month	Not reported	Upadhyay et al.[10]
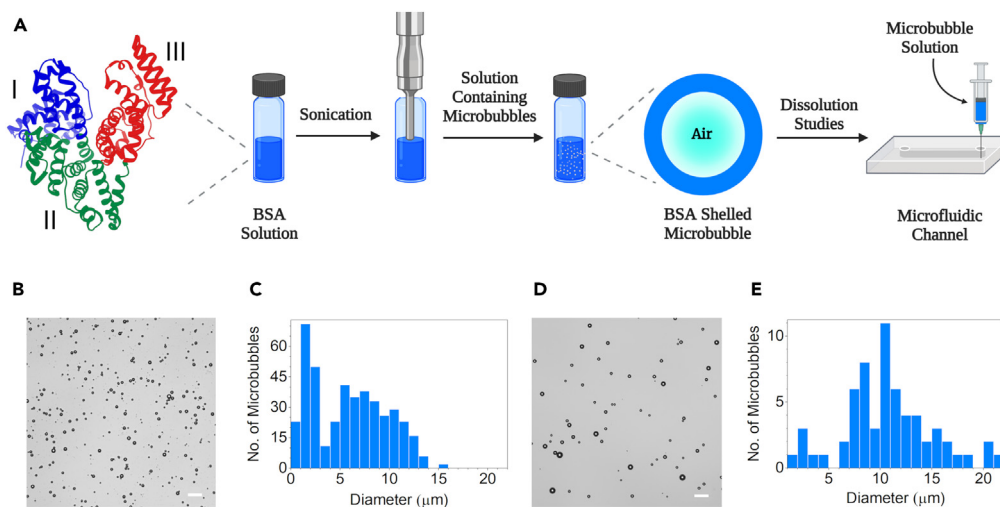
Figure 1. BSA-shelled microbubble preparation and characterization

(A) Schematic of the BSA (PDB ID: 4F5S)-shelled microbubble formation process using a probe sonicator and the microfluidic setup used for dissolution studies. Image created using: BioRender.com.

(B and C) Optical micrograph of (B) native BSA-shelled microbubbles (scale bar, 50 μm) and (C) their size distribution.

(D and E) Optical micrograph of (D) denatured BSA-shelled microbubbles (scale bar, 50 μm) and (E) their size distribution.

BSA is a heart-shaped, negatively charged protein made up of 583 amino acids, with a molecular weight of 66 kDa.[18,19] As shown in Figure 1A, the BSA structure comprises of three domains (I–III), each with two subdomains, commonly referred to as A and B, in a predominantly α-helical structure (~55%–68%). The domain I (represented in blue) contains amino acids 1–195, domain II (represented in green) contains amino acids 196–383, and domain III (represented in red) contains amino acids 384–583. This entire structure is held together by 17 uniquely linked disulfide bridges, with a pattern common to the serum albumin family of proteins.

These disulfide bonds are believed to play a vital role in the formation of microbubbles in BSA solution, although the exact mechanism of BSA shell formation during sonication is yet to be understood.[20] Many studies have highlighted the importance of the reorganization of disulfide bonds in providing stability to the protein shell. During sonication, due to acoustic cavitation in water, H· and OH· radicals are generated, which on reaction with O_2, produce HO_2 superoxide. This superoxide readily oxidizes the thiol groups of the cysteine residues of the proteins, leading to the formation of shell stabilizing intermolecular disulfide bonds.[13] This was asserted in studies involving proteins without cysteine residues, where no microbubble formations were observed.[13] There were, however, also reports that showed that proteins such as streptavidin, which also did not contain cysteine residues, assembled to form stable microbubbles without S–S bond formation, where mechanisms involving hydrophobic and H-bond interactions were believed to play crucial roles.[21] This suggests a high probability that, in the case of BSA, the microbubble shell, in addition to covalent interactions (S-S bonds), is also stabilized by short-ranged non-covalent interactions (hydrophobic and hydrophilic).[22] Also, it has been found that BSA undergoes reversible conformational changes when heated up to 45°C and subsequently cooled.[23] Between 45°C and 65°C, it undergoes partially reversible denaturation, and above this temperature, it undergoes complete irreversible denaturation, wherein the helices present in each domain starts melting, leading to the loss of secondary structure. The effect of various pre-heating temperatures on BSA microbubble stability has also been studied earlier.[16]

However, our results demonstrate that air core microbubbles created using native BSA (NBSA) remain more stable compared with those created using denatured BSA (DBSA). NBSA-shelled microbubbles have been found to be stable for over nine months at 4°C, whereas the bubbles formed using pre-heated BSA are stable for a maximum of only two days, in sealed vials. This intriguing result has been investigated in depth in the present work, as the possibility of synthesizing stable air microbubbles with native protein molecules is likely to open up new research directions pertaining to active cargo transport and biosensing under complex environments. To probe the microbubble stability in depth, we performed aging studies of native and denatured BSA-shelled microbubbles within carefully designed microfluidic channels and developed a theoretical model to predict their size-dependent shelf lives. Moreover, computational studies have also been performed to understand the changes in protein conformation upon heating, which results in higher gas leakage rates from the microbubble core.

RESULTS AND DISCUSSION

Lifetimes of microbubbles: Native vs. denatured protein

After the synthesis of BSA-shelled microbubbles as shown in Figure 1A, both native and denatured bubbles were imaged 1 h post-sonication. The corresponding microscopic images are shown in Figures 1B and 1D, with their typical size distributions in Figures 1C and 1E, respectively.
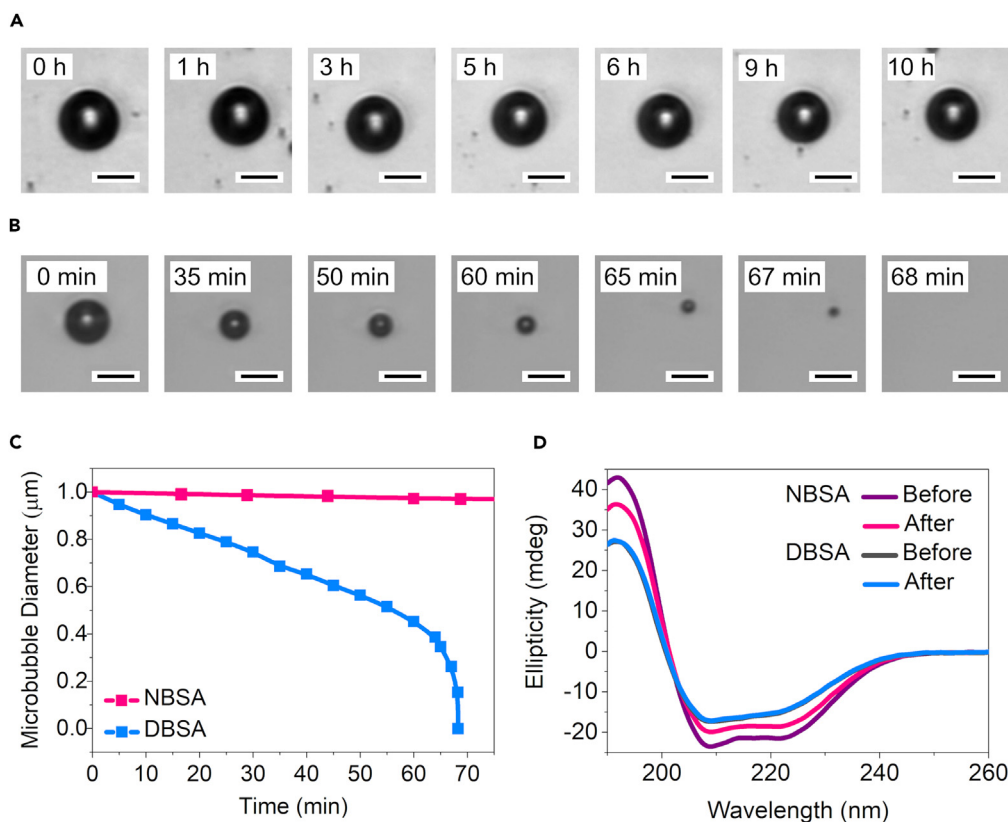
Figure 2. Single microbubble dissolution experiments reveal native BSA-coated microbubbles have markedly greater stability compared with denatured BSA-shelled microbubbles

(A and B) Microbubble dissolution snapshots for (A) native (B) denatured bubbles (scale bar, 10 μm).

(C) Comparison of normalized rates of dissolution of native and denatured bubbles.

(D) CD spectra of native and denatured BSA before and after sonication.

We notice that the number density of NBSA microbubbles is greater than DBSA bubbles and also, the samples are quite polydisperse. Detailed information about the microbubble synthesis protocol, imaging method, and post-processing of experimental data has been provided in the STAR Methods section.

There are many techniques such as differential centrifugation[24] reported for size isolation of microbubbles to obtain a narrower size distribution; however, this technique was not adapted in the present study as centrifugation resulted in microbubble samples with poor stability. Instead, we imaged as prepared single microbubbles within carefully designed microfluidic channels and monitored their time-dependent size decrement (Figures 2A and 2B).

Figure 2C shows how the sizes of both native and denatured BSA-shelled microbubbles change over time within the microfluidic channel. As time progressed, the diameter of a typical air-filled DBSA microbubble was found to decay rapidly compared with that of an NBSA bubble. When observed in the experimental chamber at 25°C, the DBSA microbubbles were found to be stable for nearly 1 h, whereas the NBSA microbubbles remained stable for more than 16 h. The time-dependent change in the diameter for microbubbles of various sizes has been provided in Figure S1 in the Supplemental Information (SI), for both NBSA and DBSA. These solutions, when stored at 4°C, displayed longer shelf lives, with denatured BSA microbubbles being stable for nearly two days and native bubbles remaining stable for more than nine months. This is consistent with the previous reports[16] of increase in microbubble stability with decreasing storage temperature. We also performed experiments to understand the stabilities and size distributions of microbubbles with varying storage temperature, sonication amplitude, sonication time, and BSA concentration. An increase in the sonication amplitude increased the number of microbubbles in the experimental solutions, along with shifting the size distribution peaks gradually toward the lower size regime. Although changes in sonication time and BSA concentration did not significantly alter the size distribution and stability of microbubbles respectively, an increase in the microbubble storage temperature led to a marked decrease in the number of bubbles within the experimental solution, within a period of nearly two days (see Figures S2–S5)

The stabilities of these microbubbles depend directly on their BSA shell morphologies, which in turn depends on the difference in protein structures at the molecular level. Hence, in order to understand the stability differences, we investigated the changes in the structure of native BSA due to heating and during high-power sonication.

Table 2. Typical % alpha helix and % beta sheet content in different BSA formulations

BSA Formulation	% Alpha helix	% Beta sheet
NBSA without sonication	65.10	6.00
NBSA with sonication	54.30	13.08
DBSA without sonication	42.85	21.30
DBSA with sonication	41.10	24.30

Secondary structure analysis

To understand the extent of conformation changes due to heating and sonication in our system, CD measurements for native and thermally denatured protein solutions were performed, as shown in Figure 2D. This "W-shaped" purple curve is the characteristic of native BSA, with the minima at 208 nm and 222 nm indicating the amount of alpha helical content. As the sample was heated, deviations from this curve were observed, indicating the unfolding and changes in secondary structures of BSA. The % helicity and beta sheet content are highlighted in Table 2.

BSA is predominantly α-helical, which is reflected in the % helicity of 65.10%. Upon heat treatment, the helicity dropped to 42.85%. Sonication also seemed to affect the helicity of BSA, although to a lesser extent (54.30% and 41.10% in NBSA and DBSA, respectively). These results indicate that the protein got slightly denatured on sonication, whereas considerable denaturation and unfolding occurred due to heat treatment.

Molecular changes in BSA structure upon thermal denaturation

In order to further understand the structural changes associated with heating BSA, we performed molecular dynamics simulations at high temperature and compared them with the room temperature native BSA simulations. Although the structural features and interaction of BSA have been studied previously using computational methods, the structure of the assembled BSA shell over microbubbles has not yet been studied, possibly due to its relatively larger size and the lack of information regarding the exact morphology of the BSA molecules surrounding the bubble. Only one study by Yeo et al. has reported the adsorption of albumin subdomains on graphene previously.[25] In recent years, theoretical methods, especially molecular dynamics (MD) simulations, have been increasingly applied to study structure-function relationships in proteins. The protein database contains several experimental data for the native BSA structure, but the structures of denatured BSA need to be generated using MD simulations. Such simulations of biomolecular systems at full atomic resolution are typically limited to the nanosecond timescale and, therefore, suffer from limited conformational sampling that cannot provide information about the exact structural changes during denaturation. Improvements in computer power and algorithms have led the state-of-the-art simulations to progress to multiple nanoseconds, so one might be tempted to think that increasing the simulation time might be able to help us overcome this challenge. However, this timescale is still too short for observing functional processes such as slow conformational changes involved in unfolding and denaturation. Hence, in this work, we performed high-temperature molecular dynamics, in a short timescale, for the conformational search of BSA upon denaturation. Such temperature-accelerated MD (TAMD) has been proven to aid in conformational searches.[26] MD of both native and denatured BSA were compared for understanding the conformational changes upon denaturation.

BSA remained stable throughout the 200 ns MD simulation at room temperature (303.15 K), with Cα RMSD fluctuating between 2 and 4 Å as compared with the initial structure (Figure 3A). The tight network of disulfide bridges has been reported to contribute to the overall stability of BSA.[27] At high temperature (500 K), the RMSD increased drastically until around 10 ns and then stabilized between 10 and 22 Å, across three independent simulations (Figure 3A).The structure of BSA can be subdivided into three domains (I, II, and III, Figure 1A). To understand the effect of thermal denaturation in these three different domains, we calculated the RMSD corresponding to these three domains separately during high temperature simulations (Figure 3B). The domain III showed the largest Cα deviations followed by domain I. Domain II was relatively the most stable during thermal denaturation. Domain III of BSA has been shown to have maximum conformational flexibility among the three domains.[19] This is due to the presence of a flexible loop in domain III, which can adopt multiple conformations. This can also be confirmed by the considerably high RMSF of domain III in both room temperature MD and high temperature MD (Figure 3C). Such a flexibility in domain III has been reported to be advantageous for certain biological functions, such as binding to fatty acids or other ligands. However, temperature-induced increased fluctuation could be detrimental to the maintenance of structural stability. Hence, in corroboration with the experimental results, it can be deduced that the heat-induced denaturation is triggered by large atomic deviations within the BSA molecule, resulting in the subsequent conformational changes in subdomains, which in turn alters the packing structure of the domains.

We further investigated the effect of thermal denaturation on the secondary structures of the BSA molecule during simulations. As expected, the room temperature simulations showed stable helical content throughout the trajectory, which also matched the helical content observed in our experimental CD studies mentioned previously. In high temperature simulations, the helical content decreases drastically within the first 10 ns, suggesting an accelerated denaturation process. In order to further select frames representing the denatured BSA, we calculated the theoretical CD spectra from frames at regular intervals from high-temperature simulations. The frames from 0 to 5 ns showed helical content in a similar range as the experimental denatured BSA solution (Figure 3D).

Further, MD-based Dictionary of Secondary Structure of Proteins (DSSP) analysis has been used in combination with CD to provide a more comprehensive picture of the temperature-induced secondary structural changes of BSA. DSSP is a program that analyzes protein structures
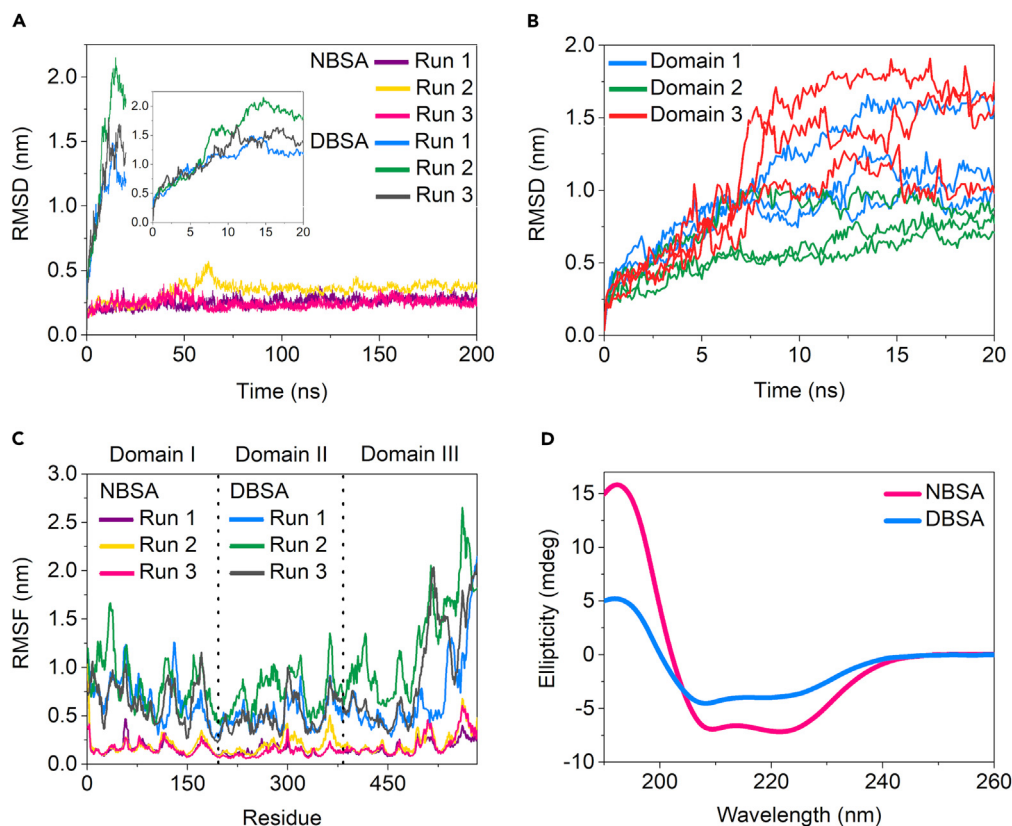
Figure 3. Simulation studies on temperature-induced conformational changes in BSA show heated protein has larger domain displacements and fluctuations

(A) RMSD of NBSA at 303.15 K and DBSA at 500 K (inset shows the RMSD of DBSA at the TAMD timescale).

(B) RMSD of domains I, II, and III of DBSA.

(C) RMSF of NBSA at 303.15 K and DBSA at 500 K.

(D) Representative CD spectra of NBSA and DBSA computed from the MD frames.

and assigns them to different secondary structure types, such as alpha helix, beta sheet, and coil. The secondary structures for BSA were maintained intact throughout the course of the standard MD, indicating a stable, native structure at 303.15 K. At high temperatures, BSA can undergo domain-specific secondary structural changes, which can affect the protein's overall stability and function. It is evident from Table 3 that BSA begins to denature and lose its alpha helical content right from the beginning of the production run. Our results corroborate with the reported studies in which domain II was found to be most stable with intact secondary structures, in comparison to domains I and III. Notably, BSA with the initial alpha-helical content of 65% denatured to 50% alpha helix within the first 5 ns and to 35% alpha helix by the end of 15 ns simulation, indicating denaturation of the protein. Specifically, the secondary structural analysis showed that B sub-domains in all three domains were more stable than the A sub-domains. In addition, our results showed that the helices accommodating the disulfide bonds of B sub-domains were found to be the most intact. Rombouts et al.[28] also observed that $(Cys)2$ residues in domains IA, IIA, and IIIA are only involved in S-S bond formation and reshuffling during thermal treatment. Based on this observation, we hypothesize that the helices of the A sub-domains are more prone to heat-induced denaturation and that they unfold and result in the reshuffling of the disulfide bonds present in them.

We next investigated the native and thermally denatured BSA molecules from the perspective of compactness and voids, which are relevant to the shell structure of microbubbles. Radius of gyration (R_g) hints toward the overall compactness of the molecules during

Table 3. % Alpha helix in the simulations of DBSA at 500 K

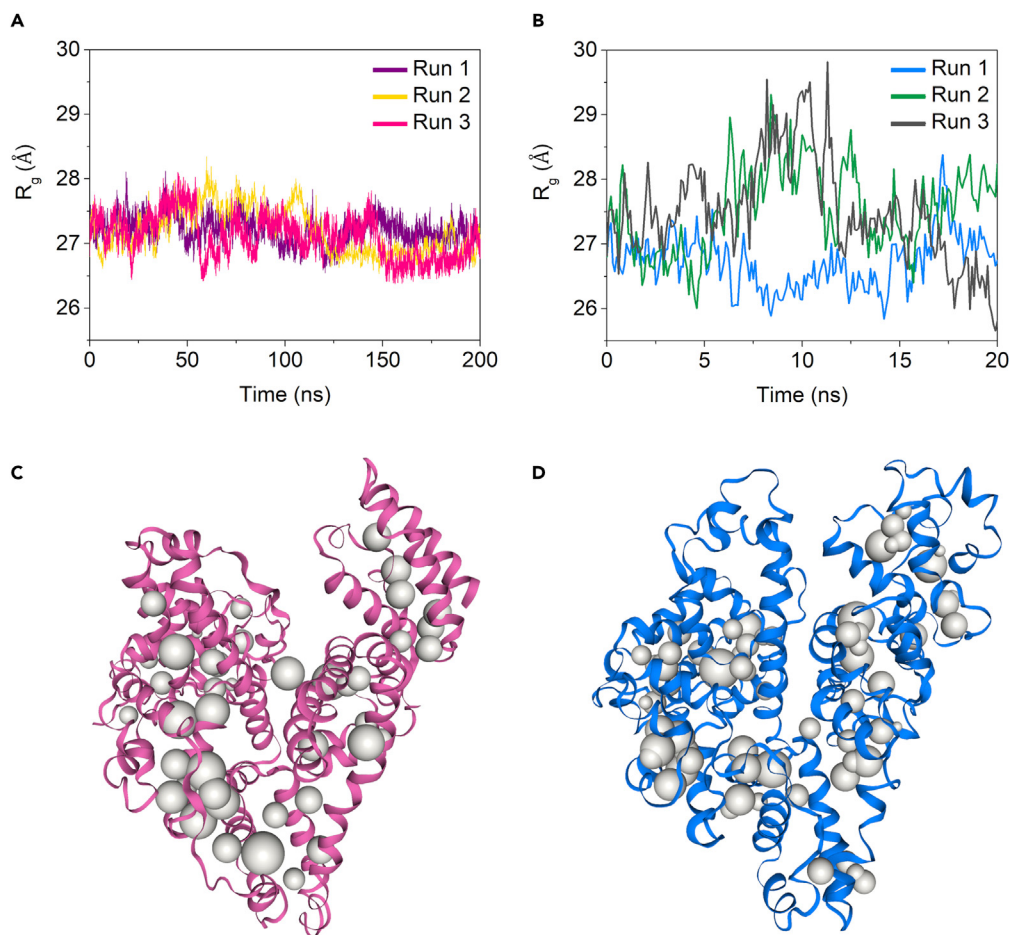| Runs	% Alpha helix at 0–5 ns	% Alpha helix at 5–10 ns	% Alpha helix at 10–15 ns
Run 1	51	39	38
Run 2	47	34	32
Run 3	53	41	37

Figure 4. Heating of BSA molecules leads to an increase in the molecular radius of gyration and a larger void volume
(A and B) Radius of gyration (R_g) of BSA at (A) 303.15 K and (B) 500 K.
(C and D) BSA structures used for calculation of void volumes of (C) NBSA and (D) DBSA.

MD simulations. We calculated R_g for room temperature, as well as for high temperature simulations. At room temperature, the R_g of BSA remained constant throughout the course of the MD simulations (Figure 4A). In case of high temperature simulations, the R_g increases during the initial stages of the simulations, indicating a decrease in the compactness and the loss of rigidity in BSA molecules (Figure 4B).

The simulations carried out in this study did not involve breaking of disulfide bonds, which might be the reason for only a modest increase in the R_g values over the course of simulations. The change in compactness can also be quantified by finding the presence of voids within the protein molecules, which will further affect the porosity of the microbubble shells, and hence, their stability. For this, we calculated the void volume in the BSA molecule using frames extracted from room-temperature and high-temperature simulations (Figures 4C and 4D). We found that the frames extracted from the high temperature simulations showed higher void volume as compared with the frames extracted from the room temperature simulations (468.78 $\pm$ 98.11 $Å^3$ vs. 299.61 $\pm$ 35.51 $Å^3$). Native BSA is a globular protein that consists of a well-defined three-dimensional structure with a hydrophobic core and hydrophilic surface residues. The interior of the protein is tightly packed with amino acid side chains, which makes it difficult for gas molecules to penetrate and diffuse within the protein structure. We hypothesize that the gas molecules can diffuse through the BSA layer, but they would not be able to penetrate into the interior of the native protein molecule. However, denatured BSA molecules that undergo structural changes and conformational fluctuations in response to changes in the surrounding environment could potentially create small pockets or voids within the protein structure that could allow gas molecules to diffuse out.

Another reason for decreased stability of the DBSA microbubbles may be attributed to the changes in the non-covalent interactions between the cross-linked protein molecules upon denaturation. As discussed earlier, the microbubble shells could be stabilized both by covalent and non-covalent interactions. Upon denaturation, some parts of protein that get melted might result in increased void volumes and higher domain fluctuations that could possibly decrease the strength of the non-covalent interactions at those locations, thereby decreasing the protein shell stability.

Estimation of gas dissolution rates from microbubbles

Microbubbles shrink in size over time due to the mass transfer of air across the protein shell from higher pressure inside the core to the surrounding medium. The pressure inside the bubble can be obtained from the Laplace equation as

$$P_2 = P_1 + \frac{2\sigma}{r} \tag{Equation 1}$$

where P_2 is the pressure inside the bubble, P_1 is the atmospheric pressure (1.01×10^5 Pa), σ is the surface tension of the microbubble surface, and r is the radius of the microbubble.

Treating the protein shell to be a tortuous porous membrane, a theoretical estimate of the bubble dissolution rate can be obtained. Assuming the size of air molecules is less than the pore size of the membrane, which is in turn less than the distance that the air molecules have to travel through the shell, we can estimate the net flux across the membrane by Knudsen diffusion:

$$J = -\frac{D}{RT}\frac{dP}{dy} = -\frac{D}{RT}\left(\frac{P_2 - P_1}{t}\right) = -\frac{D}{tRT}\frac{2\sigma}{r} \tag{Equation 2}$$

where R is the universal gas constant (8.314 J/mol K), T is the temperature (303.15 K), t is the shell thickness, and D is the Knudsen diffusion coefficient given by

$$D = \frac{d\varepsilon}{3\tau}\sqrt{\frac{8RT}{\pi M}} \tag{Equation 3}$$

where d is the pore size of the membrane, ε is the surface porosity, τ is the tortuosity, and M is the molecular weight of the diffusing gas (29 g/mol for air). Hence, Equation 2 can be written as

$$J = -\frac{4\sigma d\varepsilon}{3\tau rt}\sqrt{\frac{2}{\pi MRT}} \tag{Equation 4}$$

On the other hand, as shown by Khan et al.,[7] the flux across the membrane can also be calculated by using a mole balance approach as

$$N = -\frac{1}{A}\frac{dn}{dt'} \tag{Equation 5}$$

where A is the microbubble surface area, n is the number of moles of air inside the bubble core, and t' is the time. Assuming the air in the core to behave as an ideal gas,

$$PV = nRT \Rightarrow \left(P_1 + \frac{2\sigma}{r}\right)\left(\frac{4}{3}\pi r^3\right) = nRT \tag{Equation 6}$$

where V is the volume of the microbubble. Hence, we get

$$n = \frac{4\pi r^3 P_1}{3RT} + \frac{8\pi\sigma r^2}{3RT} \tag{Equation 7}$$

Taking the time derivative

$$\frac{dn}{dt'} = \frac{4\pi P_1}{RT}r^2\frac{dr}{dt'} + \frac{16\pi\sigma}{3RT}r\frac{dr}{dt'} + \frac{8\pi r^2}{3RT}\frac{d\sigma}{dt'} \tag{Equation 8}$$

Now, as the microbubble size continuously decreases with time, the surface tension changes as well. From the model given by de Jong et al.,[29] the variable surface tension across the bubble surface may be given as[30]

$$\sigma = \sigma_0 + E_S\left[\left(\frac{r}{r_0}\right) - 1\right] \tag{Equation 9}$$

where σ_0 is the initial surface tension, r_0 is the initial microbubble radius, and E_S is the stiffness parameter, which is a measure of the shell elasticity. Taking the time derivative of Equation 9 and solving further, we get

$$N = -\frac{1}{RT}\left[P_1 + \frac{2E_S}{r_0} + \frac{4(\sigma_0 - E_S)}{3r}\right]\frac{dr}{dt'} \tag{Equation 10}$$

Comparing Equations 4 and 10, the time rate of change of microbubble radius can be given by

$$\frac{dr}{dt'} = \frac{4d\varepsilon}{3rt\tau}\sqrt{\frac{2RT}{\pi M}} + \left[\frac{\sigma_0 + \left(\frac{r}{r_0}\right)E_S - E_S}{P_1 + \frac{2E_S}{r_0} + \frac{4(\sigma_0 - E_S)}{3r}}\right] \tag{Equation 11}$$

Table 4. Estimated shell parameter values for NBSA and DBSA microbubbles

Shell parameter	Estimated values for NBSA	Estimated values for DBSA
σ_0	35.9 (mN/m)	35.9 (mN/m)
E_S	50.1 (mN/m)	50.1 (mN/m)
d	8.30 (Å)	9.64 (Å)
ϵ	3.75×10^{-3}	5.64×10^{-3}
t	100 nm	100 nm

This expression allows us to estimate the microbubble dissolution rate in terms of the bubble shell parameters like surface tension, shell elasticity, surface porosity, tortuosity, pore size, and shell thickness. The chosen values of these parameters for native and denatured BSA are highlighted in Table 4. Due to lack of experimental data and theoretical estimates of the parameters, the following values are to be considered as rough estimations in order to understand the differences in stabilities of native and denatured protein microbubbles.

Reported values of BSA-coated microbubble shell thickness indicate ranges from 15 to 150 nm.[31] Based on this, and our experimental measurements (data not shown), we take the shell thickness to be ~100 nm, for both NBSA and DBSA. In order to find the pore size and porosity, we estimate the values of d and ϵ from our computational void volume calculations. Assuming the void per molecule to be a single sphere, we approximated its diameter and took that to be the average pore size of a single BSA molecule. By computing the total volume of NBSA and DBSA structures using the ProteinVolume webserver,[32] the porosity was calculated by taking the ratio of the void volume and total volume. From these values, it is clear that the voids in native protein are lesser compared with the denatured protein, which leads to greater gas diffusion in the latter. The surface tension and shell elasticity values for denatured BSA were obtained from the study by Khan et al.[7] Assuming that these values have the same order of magnitude for native BSA as well, the values of σ_0 and E_s are taken to be same as that of DBSA.

Now, the only adjustable parameter left is the tortuosity. It is defined as the ratio of the curved distance traveled by the gas molecule through the protein shell and the end-to-end distance. As the molecule follows a tortuous path, it is clear that the value of this parameter will always be greater than 1. Also, as the structure of native BSA is more compact compared with heated BSA, the value of τ for NBSA is expected to be greater than DBSA. Assuming it is 10 times greater, and solving Equation 11, the rate of dissolution of native BSA microbubbles turns out to be 0.057 times the dissolution rate of denatured BSA bubbles. We assume this rate to be constant throughout the dissolution period.

Now, taking the initial microbubble radius to be 6.23 μm in both the cases, we obtain the complete dissolution time for NBSA bubbles to be 17.54 times the dissolution time for DBSA microbubbles. Now, as observed in our experimental data, the DBSA microbubbles dissolve in nearly 70 min. From the theoretical model, if the dissolution time for DBSA is considered to be the same, then the corresponding NBSA dissolution time should be around 20 h, which matches well with our experimental observations.

This analytical model for gas dissolution, under the given set of assumptions, also suggests that native protein-shelled microbubbles are more stable compared with the denatured protein bubbles. We, however, also need to note that the microbubble dissolution will depend not only on the tortuosity of the protein shell but also on other factors that have not been included in our model. It is also likely that the air molecules might get trapped in various micro-voids inside the shell before diffusing out, as reported for polymers,[33] or they might also face additional hindrance in permeability due to the gas barrier properties of proteins.[34–36] Native BSA being more compact, it might lead to larger gas trapping. It has also been observed that when air traverses a more tortuous path, the oxygen molecules form "temporary" hydrogen bonds with the hydroxyl groups of the protein film, thus leading to a "dragging" effect, which leads to reduction in gas permeability.[37] All these factors together can lead to larger differences in the gas permeation rates through the microbubble shell, thus amounting to the considerable difference in NBSA and DBSA microbubble stabilities.

To summarize, we investigated the enhanced stability of air-filled, native BSA-coated microbubbles over those synthesized using denatured BSA. It was found that while air core, DBSA bubbles remained stable for two days at 4°C, NBSA bubbles were stable for more than nine months. By performing single-microbubble dissolution studies at room temperature under microfluidic environments, bubble lifetimes were characterized. Molecular dynamics simulations were also carried out to understand the protein structural change on heating, by observing the root-mean-square deviation and fluctuation of the three protein domains. Furthermore, by studying the radius of gyration of the NBSA and DBSA, the voids within the protein molecules were compared. It was found that the radius of gyration of DBSA was larger, resulting in its greater void volume. From these results we concluded that as BSA was heated, the molecule lost its compactness, and hence, when microbubble shells were formed with denatured BSA assemblies, the volume of voids within and between the molecules was larger, leading to faster gas leakage rates from the bubble core. Finally, we presented a theoretical model for predicting the bubble dissolution rate dependent on its shell parameters. These results are expected to enable researchers to design microbubble-based smart payload carriers whose stability can be tuned by changing the degree of nativity of its shell-forming protein.

Limitations of the study

Our study uses bovine serum albumin as a microbubble shell coating, the biocompatibility of which has been a subject of deliberation.[10,20] For *in vivo* applications, these microbubbles need to be further checked for their biocompatibility, integrability, and immunogenic response

triggered in the host. With our simulation studies, we were able to conclude that when BSA molecule was heated, its domain fluctuations increased, leading to larger void volumes within the molecule. The larger voids led to greater gas diffusion rates through the molecule. However, the exact mechanism of shell formation by BSA molecules and the process of gas diffusion through a layer of multiple proteins need to be understood in detail to gain a comprehensive insight into the stability of protein-shelled microbubbles.

STAR★METHODS

Detailed methods are provided in the online version of this paper and include the following:

- KEY RESOURCES TABLE
- RESOURCE AVAILABILITY
  - Lead contact
  - Materials availability
  - Data and code availability
- METHOD DETAILS
  - Microbubble synthesis
  - Chamber preparation
  - Optical microscopy
  - Secondary structure measurements
  - Molecular dynamics simulations
  - Calculation of void volume

SUPPLEMENTAL INFORMATION

Supplemental information can be found online at https://doi.org/10.1016/j.isci.2024.109286.

AUTHOR CONTRIBUTIONS

P.D. and N.S. developed protocols, designed experiments, collected and analyzed data, and wrote the paper. These authors contributed equally. V.S. and A.S. performed computational studies and contributed to manuscript writing. A.A.S., Y.M., and D.A.G. helped in data analysis and manuscript writing. K.K.D. conceptualized, and supervised the project and helped in manuscript writing.

DECLARATION OF INTERESTS

The authors declare no competing interests.

REFERENCES

1. Gramiak, R., and Shah, P.M. (1968). Echocardiography of the Aortic Root. Invest. Radiol. 3, 356–366. https://doi.org/10.1097/00004424-196809000-00011.

2. Blomley, M.J.K., Cooke, J.C., Unger, E.C., Monaghan, M.J., and Cosgrove, D.O. (2001). Microbubble contrast agents: a new era in ultrasound. Br. Med. J. 322, 1222–1225. https://doi.org/10.1136/bmj.322.7296.1222.

3. Sirsi, S., and Borden, M.A. (2009). Microbubble Compositions, Properties and Biomedical Applications. Bubble Sci. Eng. Technol. 1, 3–17. https://doi.org/10.1179/175889709X446507.

4. Kwan, J.J., Kaya, M., Borden, M.A., and Dayton, P.A. (2012). Theranostic Oxygen Delivery Using Ultrasound and Microbubbles. Theranostics 2, 1174–1184. https://doi.org/10.7150/thno.4410.

5. Tsutsui, J.M., Xie, F., and Porter, R.T. (2004). The use of microbubbles to target drug delivery. Cardiovasc. Ultrasound 2. https://doi.org/10.1186/1476-7120-2-23.

6. Park, B., Yoon, S., Choi, Y., Jang, J., Park, S., and Choi, J. (2020). Stability of Engineered Micro or Nanobubbles for Biomedical Applications. Pharmaceutics 12, 1089. https://doi.org/10.3390/pharmaceutics12111089.

7. Khan, A.H., and Dalvi, S.V. (2020). Kinetics of albumin microbubble dissolution in aqueous

media. Soft Matter *16*, 2149–2163. https://doi.org/10.1039/C9SM01516G.

8. Sarkar, K., Katiyar, A., and Jain, P. (2009). Growth and Dissolution of an Encapsulated Contrast Microbubble: Effects of Encapsulation Permeability. Ultrasound Med. Biol. *35*, 1385–1396. https://doi.org/10.1016/j.ultrasmedbio.2009.04.010.

9. Kwan, J.J., and Borden, M.A. (2010). Microbubble Dissolution in a Multigas Environment. Langmuir *26*, 6542–6548. https://doi.org/10.1021/la904088p.

10. Upadhyay, A., Dalvi, S.V., Gupta, G., and Khanna, N. (2017). Effect of PEGylation on performance of protein microbubbles and its comparison with lipid microbubbles. Mater. Sci. Eng. C *71*, 425–430. https://doi.org/10.1016/j.msec.2016.10.021.

11. Upadhyay, A., and Dalvi, S.V. (2016). Synthesis, characterization and stability of BSA-encapsulated microbubbles. RSC Adv. *6*, 15016–15026. https://doi.org/10.1039/C5RA24304A.

12. Grinstaff, M.W., and Suslick, K.S. (1991). Air-filled proteinaceous microbubbles: synthesis of an echo-contrast agent. Proc. Natl. Acad. Sci. USA *88*, 7708–7710. https://doi.org/10.1073/pnas.88.17.7708.

13. Suslick, K.S., Grinstaff, M.W., Kolbeck, K.J., and Wong, M. (1994). Characterization of sonochemically prepared proteinaceous microspheres. Ultrason. Sonochem. *1*, S65–S68. https://doi.org/10.1016/1350-4177(94)90030-2.

14. Swanson, E.J., and Borden, M.A. (2010). Injectable Oxygen Delivery Based on Protein-Shelled Microbubbles. Nano Life *01*, 215–218. https://doi.org/10.1142/S1793984410000195.

15. Borrelli, M.J., O'Brien, W.D., Jr., Bernock, L.J., Williams, H.R., Hamilton, E., Wu, J., Oelze, M.L., and Culp, W.C. (2012). Production of uniformly sized serum albumin and dextrose microbubbles. Ultrason. Sonochem. *19*, 198–208. https://doi.org/10.1016/j.ultsonch.2011.05.010.

16. Rovers, T.A.M., Sala, G., van der Linden, E., and Meinders, M.B.J. (2016). Temperature is key to yield and stability of BSA stabilized microbubbles. Food Hydrocolloids *52*, 106–115. https://doi.org/10.1016/j.foodhyd.2015.05.038.

17. Ma, X., Bussonniere, A., and Liu, Q. (2017). A facile sonochemical synthesis of shell-stabilized reactive microbubbles using surface-thiolated bovine serum albumin with the Traut's reagent. Ultrason. Sonochem. *36*, 454–465. https://doi.org/10.1016/j.ultsonch.2016.12.033.

18. Topală, T., Bodoki, A., Oprean, L., and Oprean, R. (2014). Bovine serum albumin interactions with metal complexes. Clujul Med. *87*, 215–219. https://doi.org/10.15386/cjmed-357.

19. Bujacz, A. (2012). Structures of bovine, equine and leporine serum albumin. Acta Crystallogr. D *68*, 1278–1289. https://doi.org/10.1107/S0907444912027047.

20. Rudakovskaya, P.G., Barmin, R.A., Kuzmin, P.S., Fedotkina, E.P., Sencha, A.N., and Gorin, D.A. (2022). Microbubbles Stabilized by Protein Shell: From Pioneering Ultrasound Contrast Agents to Advanced Theranostic Systems. Pharmaceutics *14*, 1236. https://doi.org/10.3390/pharmaceutics14061236.

21. Avivi, S., and Gedanken, A. (2002). S-S bonds are not required for the sonochemical formation of proteinaceous microspheres: the case of streptavidin. Biochem. J. *366*, 705–707. https://doi.org/10.1042/BJ20020676.

22. Cavalieri, F., Ashokkumar, M., Grieser, F., and Caruso, F. (2008). Ultrasonic Synthesis of Stable, Functional Lysozyme Microbubbles. Langmuir *24*, 10078–10083. https://doi.org/10.1021/la801093q.

23. Takeda, K., Wada, A., Yamamoto, K., Moriyama, Y., and Aoki, K. (1989). Conformational change of bovine serum albumin by heat treatment. J. Protein Chem. *8*, 653–659. https://doi.org/10.1007/BF01025605.

24. Feshitan, J.A., Chen, C.C., Kwan, J.J., and Borden, M.A. (2009). Microbubble size isolation by differential centrifugation. J. Colloid Interface Sci. *329*, 316–324. https://doi.org/10.1016/j.jcis.2008.09.066.

25. Yeo, J.J., Han, Y.T., and Cheng, Y. (2015). Conformational change of an α-helix segment of bovine serum albumin adsorbed on graphene. International Conference on Composite Materials, Auckland, New Zealand. https://www.sci-en-tech.com/ICCM2015/PDFs/704-2912-1-PB.pdf.

26. Abrams, C.F., and Vanden-Eijnden, E. (2010). Large-scale conformational sampling of proteins using temperature-accelerated molecular dynamics. Proc. Natl. Acad. Sci. USA *107*, 4961–4966. https://doi.org/10.1073/pnas.0914540107.

27. Brandt, N.N., Chikishev, A.Y., Mankova, A.A., and Sakodynskaya, I.K. (2014). Effect of thermal denaturation, inhibition, and cleavage of disulfide bonds on the low-frequency Raman and FTIR spectra of chymotrypsin and albumin. J. Biomed. Opt. *20*, 051015. https://doi.org/10.1117/1.JBO.20.5.051015.

28. Rombouts, I., Lagrain, B., Scherf, K.A., Lambrecht, M.A., Koehler, P., and Delcour, J.A. (2015). Formation and reshuffling of disulfide bonds in bovine serum albumin demonstrated using tandem mass spectrometry with collision-induced and electron-transfer dissociation. Sci. Rep. *5*, 12210. https://doi.org/10.1038/srep12210.

29. de Jong, N., Hoff, L., Skotland, T., and Bom, N. (1992). Absorption and scatter of encapsulated gas filled microspheres: Theoretical considerations and some measurements. Ultrasonics *30*, 95–103. https://doi.org/10.1016/0041-624X(92)90041-J.

30. Helfield, B. (2019). A Review of Phospholipid Encapsulated Ultrasound Contrast Agent Microbubble Physics. Ultrasound Med. Biol.

45, 282–300. https://doi.org/10.1016/j.ultrasmedbio.2018.09.020.

31. Navarro-Becerra, J.A., and Borden, M.A. (2023). Targeted Microbubbles for Drug, Gene, and Cell Delivery in Therapy and Immunotherapy. Pharmaceutics *15*, 1625. https://doi.org/10.3390/pharmaceutics15061625.

32. Chen, C.R., and Makhatadze, G.I. (2015). ProteinVolume: calculating molecular van der Waals and void volumes in proteins. BMC Bioinf. *16*, 101. https://doi.org/10.1186/s12859-015-0531-2.

33. Vieth, W.R., and Sladek, K.J. (1965). A Model for Diffusion in a Glassy Polymer. J. Colloid Sci. *20*, 1014–1033. https://doi.org/10.1016/0095-8522(65)90071-1.

34. Cuq, B., Gontard, N., and Guilbert, S. (1998). Proteins as Agricultural Polymers for Packaging Production. Cereal Chem. *75*, 1–9. https://doi.org/10.1094/CCHEM.1998.75.1.1.

35. Guilbert, S., Cuq, B., and Gontard, N. (1997). Recent Innovations in Edible and/or Biodegradable Packaging Materials. Food Addit. Contam. *14*, 741–751. https://doi.org/10.1080/02652039709374585.

36. Bibi, F., Guillaume, C., Gontard, N., and Sorli, B. (2017). Wheat gluten, a bio-polymer to monitor carbon dioxide in food packaging: Electric and dielectric characterization. Sensor. Actuator. B Chem. *250*, 76–84. https://doi.org/10.1016/j.snb.2017.03.164.

37. Sun, B., Wang, W., Zhang, M., and Sain, M. (2018). Biomass-based edible film with enhanced mass barrier capacity and gas permeable selectivity. Cellulose *25*, 5919–5937. https://doi.org/10.1007/s10570-018-1976-z.

38. Abraham, M.J., Murtola, T., Schulz, R., Páll, S., Smith, J.C., Hess, B., and Lindahl, E. (2015). GROMACS: High performance molecular simulations through multi-level parallelism from laptops to supercomputers. SoftwareX *1–2*, 19–25. https://doi.org/10.1016/j.softx.2015.06.001.

39. Drew, E.D., and Janes, R.W. (2020). PDBMD2CD: providing predicted protein circular dichroism spectra from multiple molecular dynamics-generated protein structures. Nucleic Acids Res. *48*, W17–W24. https://doi.org/10.1093/nar/gkaa296.

40. Staritzbichler, R., Ristic, N., Goede, A., Preissner, R., and Hildebrand, P.W. (2021). Voronoia 4-ever. Nucleic Acids Res. *49*, W685–W690. https://doi.org/10.1093/nar/gkab466.

41. Lindorff-Larsen, K., Piana, S., Palmo, K., Maragakis, P., Klepeis, J.L., Dror, R.O., and Shaw, D.E. (2010). Improved side-chain torsion potentials for the Amber ff99SB protein force field. Proteins *78*, 1950–1958. https://doi.org/10.1002/prot.22711.

42. Hess, B., Bekker, H., Berendsen, H.J.C., and Fraaije, J.G.E.M. (1997). LINCS: A linear constraint solver for molecular simulations. J. Comput. Chem. *18*, 1463–1472. https://doi.org/10.1002/(SICI)1096-987X(199709)18:12<1463::AID-JCC4>3.0.CO;2-H.

STAR★METHODS

KEY RESOURCES TABLE

REAGENT or RESOURCE	SOURCE	IDENTIFIER
Chemicals, peptides, and recombinant proteins		
Bovine Serum Albumin	Sigma Aldrich, USA	CAS: 9048-46-8
Software and algorithms		
ImageJ	National Institutes of Health	https://imagej.nih.gov/ij/
GROMACS	Abraham et al.[38]	https://www.gromacs.org/
PDBMD2CD	Drew et al.[39]	https://pdbmd2cd.cryst.bbk.ac.uk/
Voronoia	Staritzbichler et al.[40]	https://proteinformatics.uni-leipzig.de/voronoia/

RESOURCE AVAILABILITY

Lead contact

Further information and requests for resources should be directed to, and will be fulfilled by the lead contact, Dr. Krishna K. Dey (k.dey@iitgn.ac.in).

Materials availability

This study did not generate any new unique reagents.

Data and code availability

- Microscopy and circular dichroism spectroscopy data reported in this paper will be shared by the lead contact upon request.
- The parameters of simulations have been described in the STAR Methods section. The compressed trajectories will be shared by the lead contact upon request.
- Any additional information required to reanalyze the data reported in this paper will be available from the lead contact upon request.

METHOD DETAILS

Microbubble synthesis

All experiments were performed using 5% w/v BSA ($\geq$ 98% lyophilized powder). The required amount of BSA (50 mg/mL) was dissolved in the necessary volume of deionized water (Direct-Q 8-UV, Merck), stirred at room temperature (25°C) for 2 h using a magnetic stirrer, and preserved at 4°C overnight. The resulting solution was then directly used to produce native BSA shelled microbubbles (NBSA). In order to synthesize microbubbles with denatured BSA (DBSA), the native solution was further heated and stirred at 75°C for 10 min, prior to preservation at 4°C. Both these solutions were then sonicated using an ultrasonic probe sonicator (Qsonica, 500 W) to generate protein shelled microbubbles. By positioning the probe tip at the air-liquid interface, the sonicator was operated at 20 kHz frequency and 60% amplitude for 2.5 min. Immediately after, the microbubbles thus produced were air sealed and rapidly cooled in an ice bath for 30 min, beyond which they were preserved at 4°C.

Chamber preparation

Dissolution studies of microbubbles over time were carried out inside a PDMS microchannel with 200 μm diameter and 4 cm length. After flowing deionized water through the chamber, the microbubble solutions were injected with a syringe and left undisturbed.

Optical microscopy

All microbubble samples were imaged and recorded in a deionized water environment, at room temperature, using an inverted optical microscope (Nikon Eclipse Ti2, Japan). After loading the sample in the microfluidic channel as described previously, single microbubble dissolutions were recorded using a high-resolution camera (Hamamatsu C13440) at 7.5 frames per second (fps) till they completely dissolved. Further image analysis was performed using ImageJ software to find the exact sizes of the microbubbles and its variation over time.

Secondary structure measurements

The stabilities of native and denatured BSA shelled microbubbles depend heavily on the protein shell morphologies, which in turn depends on the secondary structures of the proteins. In order to understand the changes in the protein secondary structures during heating, Circular

Dichroism (CD) spectroscopy (JASCO J 815) was used. 2 μM solutions of BSA were prepared and used in experiments. The samples were scanned in a 1 mm path length cell, in the wavelength range of 190-320 nm, with 1 nm bandwidth and 3 accumulations during each run, at room temperature. Each sample was tested 3 times to estimate the statistical uncertainties. The data obtained was then analyzed using the JASCO Secondary Structure Estimation software to find the % alpha helix and % beta sheet in different BSA formulations.

Molecular dynamics simulations

Using the crystal structure of BSA obtained from the Protein Data Bank (ID: 4F5S),[19] the structure and dynamics of BSA were investigated using atomistic MD simulations through GROMACS (GROningen MAchine for Chemical Simulations)[38,41] version 2021.2. The Amber ff99SB-ILDN force field[41] was used for the protein and TIP4P was used as a water model. The crystal structure of BSA was solvated in a dodecahedron box with the appropriate water model and force field, followed by the addition of sodium (Na^+) and chloride (Cl^-) ions to make the system charge neutral. MD simulations were performed at constant temperature, pressure and number of particles (NPT ensemble). Protein and non-protein atoms were coupled to their own temperature baths, which were kept constant at either 303.15 K (standard MD) or 500 K [temperature accelerated MD (TAMD)], using the weak coupling algorithm. The pressure was maintained isotropically at 1 bar using the Berendsen barostat. Prior to the production runs, the energy of each system was minimized using the steepest descents method. This was followed by 100 ps of position restrained dynamics, with all non-hydrogen atoms restrained with a 1000 kJ/mol force constant in an NVT ensemble.

Subsequently, the system was equilibrated in an NPT ensemble for 10 ns, where the pressure was maintained at 1 bar using a Berendsen barostat. The NVT and NPT equilibrations were followed by production runs of 200 ns for a standard MD simulation or 20 ns for a TAMD, in an NPT ensemble using a Parinello-Rahman barostat and modified Berendsen Thermostat (V-rescale), with the temperature maintained at 303.15 K or 500 K and pressure at 1 bar. Three independent simulations were performed for each of the systems. The timestep was set to 2 fs. Initial atom velocities were taken from a Maxwellian distribution at 303.15 K or 500 K. All bond lengths were constrained using the LINCS algorithm.[42] Periodic boundary conditions were applied in all directions. The obtained trajectories were then analyzed using in-built functions of GROMACS. Root mean square deviation (RMSD), root mean square fluctuation (RMSF), radius of gyration (Rg), and secondary structures were calculated using gmx rmsd, gmx rmsf, gmx gyration and gmx dssp functions of GROMACS, respectively. Discovery studio visualizer, Pymol, and VMD were used for molecular visualization. Theoretical computation of the CD spectra of the protein structures generated by MD was performed using the PDBMD2CD webserver.[39]

Calculation of void volume

The void volumes in the frames corresponding to room temperature and high temperature simulations were calculated using Voronoia web tool.[40] Voronoia uses Delaunay triangulation to find cavities within the protein molecule. Six frames were chosen from three different trajectories of high temperature simulations between 5 and 10 ns for void volume calculation. Similarly, six frames were randomly chosen from the room temperature simulations to calculate the void volume in native BSA. The volume of each sphere placed in the cavities of the proteins was calculated using the radius provided by the Voronoia web tool.